Nano Research 2016, 9(7): 2097–2109
DOI 10.1007/s12274-016-1100-3
Research Article
ISSN 1998-0124
CN 11-5974/O4

An *in vivo* study of the biodistribution of gold nanoparticles after intervaginal space injection in the tarsal tunnel

Xiaoli Shi[1], Yuting Zhu[1], Wenda Hua[1], Yinglu Ji[1], Qing Ha[1], Xinxiao Han[1], Yang Liu[1], Jingwei Gao[1], Qiang Zhang[1], Sidi Liu[1], Keli Ren[1], Xiaochun Wu[1], Hongyi Li[2] (✉), and Dong Han[1] (✉)

[1] *National Center for Nanoscience and Technology, Beijing 100190, China*
[2] *Cardiology Division, Beijing Hospital of the Ministry of Health, Beijing 100730, China*

Received: 18 September 2015
Revised: 10 April 2016
Accepted: 14 April 2016

KEYWORDS

gold nanospheres, hierarchical multiphase porous medium, intervaginal space injection, *in vivo* transport, inductively coupled plasma mass spectrometry (ICP-MS)

ABSTRACT

The biodistribution of gold nanoparticles (AuNPs) is closely related to toxicological effects and is of great concern because of their potential application in diverse biomedical areas. However, with the discovery of novel anatomic and histological structures for fluid transport, the underlying mechanisms involved in the *in vivo* transport and biodistribution of AuNPs require further in-depth investigations. In the current study, we investigated the biodistribution of 10-nm AuNPs in rats after intervaginal space injection (ISI) in the tarsal tunnel, where a focal point of tendons, vessels, and nerve fibers may optimally connect to other remote connective tissues. The intravenous injection (IVI) of AuNPs served as a control. The blood and organs were collected at 5, 15, and 30 min and at 1, 4, 12, and 24 h after injection for quantitative analysis of Au distribution with inductively coupled plasma mass spectrometry (ICP-MS). IVI and ISI yielded significantly different results: The AuNP content in the blood after ISI was much lower than that after IVI; was similar in the lungs, heart, and intestines; and was higher in the skin and muscle. These findings were supported by the ratios of AuNP content and relative organ AuNP distribution proportions. Our results demonstrated a fast, direct, and the circulation-independent AuNP–organ transport pathway, which may improve our understanding of physiological and pathological biodistribution processes in biological systems. Furthermore, these results provide novel insights into the *in vivo* transport and biodistribution of AuNPs, which may lead to novel and efficient therapeutic and administration strategies.

Address correspondence to Dong Han, dhan@nanoctr.cn; Hongyi Li, leehongyi@nanoctr.cn

1 Introduction

During the last decade, nanotechnology and nanoscience have matured significantly in multidisciplinary fields, and have thus been used in electronic components, sports equipment, and biomedical applications [1–4]. As a model particle for nanotechnology research, gold nanoparticles (AuNPs), which possess diverse advantageous properties including a unique synthesis profile, controllable surface chemistry, localized surface plasmon resonance, and biocompatibility, are actively used in numerous biomedical applications, such as cell imaging, biosensors, targeted drug delivery, diagnostics, and therapeutics [4–6]. Currently, several AuNP-based drugs are under investigation in ongoing clinical trials [7–9]. The use of AuNPs in medicine raises critical questions about their transport, biodistribution, and potential toxicity to an organism, all of which should be rigorously investigated before clinical use.

In the past few years, there has been a substantial increase in research into the biodistribution and toxic effects of NPs *in vivo*, which have been evaluated under a range of experimental conditions such as different dosages, administration routes, and particle concentrations, as well as using NPs with different properties including different sizes, shapes, surface functionalizations, and aggregation profiles [9–11]. Because of the wide variety of experimental conditions tested, there is a large amount of data on the biodistribution and toxicity of NPs. For example, De Jong et al. studied the influence of AuNP size (10, 50, 100, and 250 nm) on particle biodistribution at 24 h after intravenous injection (IVI) into rats using inductively coupled plasma mass spectrometry (ICP-MS). They found that the tissue distribution of AuNPs was size-dependent with the majority of the particles distributed to the liver and spleen [12]. Zhang et al. compared the *in vivo* toxicity of three different administration routes of 13.5-nm AuNPs in mice and showed that oral administration and intraperitoneal injection (IPI) resulted in the highest toxicity, whereas tail vein injection resulted in the lowest toxicity [13]. Wang et al. quantitatively investigated the biodistribution of Au nanorods at different time points in Sprague-Dawley (SD) rats after IVI using ICP-MS. Their results indicated that AuNPs had a fast blood clearance rate and that most of the particles were transported to the liver, followed by the spleen and lungs [14]. Hillyer and Albrecht studied the gastrointestinal uptake and subsequent organ distribution of nanometer-sized AuNPs following oral administration to mice. They found that smaller colloidal AuNPs were able to cross the gut mucosa and localize to tissues more readily than larger AuNPs, with high levels observed in the small intestine and stomach [15].

The effects of the administration route of NPs on their biodistribution have been discussed in detail [13, 15]. IVI, IPI, subcutaneous injection, transdermal, inhalation, and oral administration are the six principal administration routes [16]. No matter the pathway used, NPs migrate into the circulation first after initial absorption, and subsequently distribute to the tissues and organs, which means that NPs mainly distribute by passive targeting. Compared to other administration routes, the IVI route has been used most frequently with the lowest toxicity [9, 13]. After IVI, the surfaces of NPs are rapidly covered by selective blood plasma proteins forming a so-called "protein corona" which can influence the properties of NPs and change their fate and biodistribution in the body. For other routes of administration, NPs must first pass through additional physiological barriers such as the skin and lungs before entering the circulation. Following differences in initial absorption due to NP size, dose, and administration route, the circulation can distribute the particles to organs and tissues throughout the body, where the majority tends to accumulate in the liver and spleen, affecting the distribution and content of NPs to targeted organs.

In addition to the circulation biodistribution pathway, other pathways may be involved in the biodistribution of NPs. Previously, we found that loose connective tissues separated from the blood or lymphatic vessels provide potential drainage systems. Specifically, we discovered that paramagnetic Gd-DTPA or fluorescein sodium that was injected into the KI3 acupuncture point of rats was transported through the venous adventitia, but not intravascularly [17]. We also injected three types of imaging tracers into healthy volunteers to visualize transport pathways using magnetic resonance imaging, X-ray, and computerized tomography. Our findings suggested that specific anatomical structures within the subcutaneous

tissues or the partial walls of certain veins were not vascular conduits, but rather represented unique fast transport pathways in humans [18]. On the basis of the observed fast tracer transport in the loose connective tissues of living systems, we prepared an artificial hierarchical multiphase porous medium *in situ* with a micrometer-scale hydrophobic fiber network filled with a nanometer-scale hydrophilic porous medium to explore the mechanism of this transport pathway [19]. We also studied the effects of the characteristics of hierarchical multiphase porous media on this transport capability (unpublished data). Our data provided strong evidence that the phenomenon was based on the nano-confined air/water/solid interface around the micrometer-scale hydrophobic fibers.

Our previous studies have been based on small soluble molecules, such as fluorescein sodium and Gd-DTPA. Therefore, to determine whether this unique pathway could transport NPs, we chose AuNPs as model substrate in the current study, and investigated the biodistribution of AuNPs after intervaginal space injection (ISI) in the tarsal tunnel, which is a method we have used earlier [17, 18]. This injection point is at a gap in the tendon bundles, which consist of connective tissue. Rats injected with a suspension containing 10-nm diameter AuNPs via ISI were compared to rats that had received the suspension via IVI into the femoral vein (control group). We chose AuNPs because of their potential medical applications and their straightforward detection without background signals. ICP-MS is one of the most sensitive techniques for trace element analysis with a large dynamic range and low detection limits [9]. Thus, ICP-MS was used here to quantitatively measure the content of AuNPs in various tissues and blood at different time points after treatment. The results reported herein may improve upon and provide novel understanding of the biodistribution and transport of AuNPs *in vivo*, and may offer a potential pathway for advanced and efficient therapeutic and diagnostic strategies.

2 Experimental

2.1 Preparation and characterization of the AuNPs

AuNPs (10 nm in diameter) were synthesized following known procedures [20]. Briefly, cetyltrimethylammonium bromide (CTAB)-capped Au seeds were synthesized by chemical reduction of $HAuCl_4$ with $NaBH_4$. Subsequently, the seed solution was added to the growth solution, which consisted of CTAB (0.1 M, 500 mL), $HAuCl_4$ (23.8 mM, 5.25 mL), and ascorbic acid (0.1 M, 75 mL), to initiate the growth of the AuNPs.

For size and shape characterization, the AuNPs were dispersed in deionized water, dripped, dried, and observed by transmission electron microscopy (TEM; G-2 transmission electron microscope, FEI Tecnai, Hillsboro, OR, USA).

2.2 Uptake by quantitative analysis

Male 6-week-old SD rats were purchased from Beijing Vital River Experimental Animal Corporation (Beijing, China). As shown in Fig. 1(a), the rats were divided into IVI (femoral vein-injected control) and ISI groups consisting of seven rats each with one injection time point. ISI was performed by injection in the tarsal tunnel on the left ankle bone [17]. The tarsal tunnel is located at the posteromedial side of the ankle and is formed by the medial malleolus of the tibia, the medial and posterior surfaces of the talus, the medial surface of the calcaneus, and the inferior surface of the sustentaculum tali of the calcaneus. There are tendon bundles, the tibial artery, and the tibial nerve located in the tarsal tunnel, which is covered by the flexor retinaculum as a strap-like layer of connective tissue. The injection point is at the gap of the tendon bundles in the tarsal tunnel [21].

The rats were weighed and anesthetized with 3.5% chloral hydrate (10 $mL \cdot kg^{-1}$ body) via IPI. Then, the rats were injected with 500 μL of an AuNP suspension at a dose of 2 $mg \cdot kg^{-1}$ body weight using 1 mL syringes (B. Braun Medical, Shanghai, China) [9]. Blood samples were then collected from the celiac artery at 5 min, 15 min, 30 min, 1 h, 4 h, 12 h, and 24 h. As shown in Fig. 1(b), the heart, liver, spleen, lungs, kidneys, intestines, and right leg muscle tissue and skin were excised and washed thoroughly with phosphate-buffered saline (PBS) to remove residual blood. After the residual water on the organ surface had been removed with filter paper, each sample was weighed and digested for quantitative analysis of the AuNPs

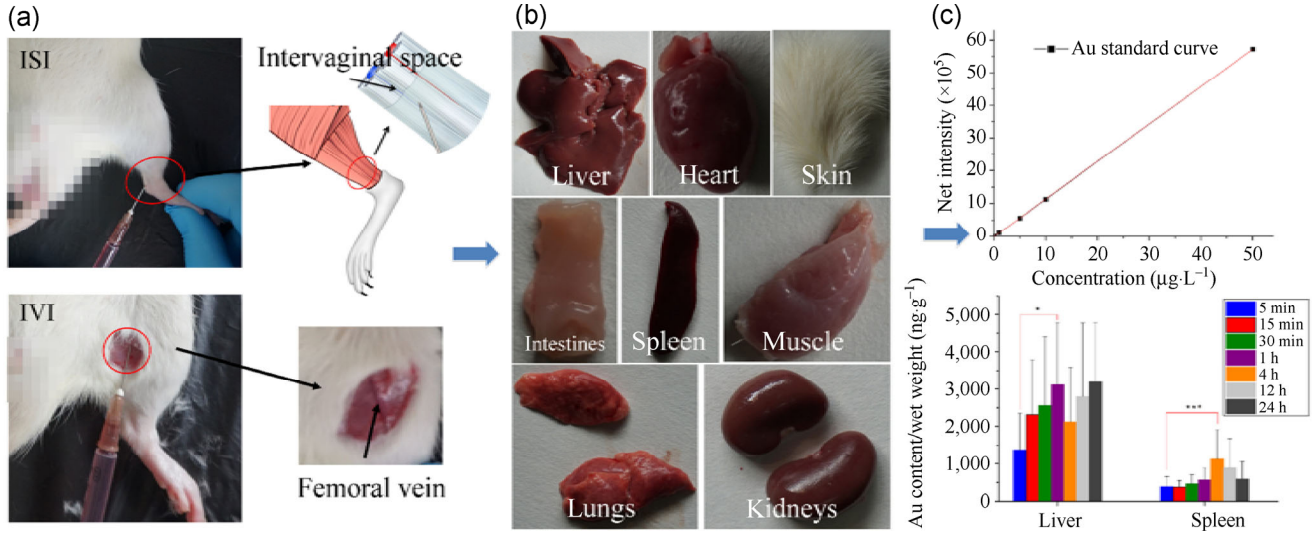

Figure 1 Experimental workflow used in this study. (a) The points of ISI into the tarsal tunnel (upper) and IVI into the femoral vein control (lower). (b) The heart, liver, spleen, lungs, kidneys, intestines, and leg muscle tissue and skin were excised. (c) ICP-MS was used to measure the gold content in each organ. A calibration curve was created using a purchased Au standard (upper), and the Au content of each tissue at each time point is represented as the means ± S.D. (lower).

by ICP-MS (Fig. 1(c)). Briefly, the samples were placed in separate beakers and were predigested with aqua regia (3 mL) overnight, followed by digestion with HNO_3 and H_2O_2 (3:1 v/v) on a hot plate for several hours. The remaining solution was cooled and diluted to 3 mL with an acid solution containing 2% HNO_3 and 1% HCl. A blank solution and a series of Au standard solutions (0.5, 1, 5, 10, and 50 ppb) diluted in the acid solution were used during the ICP-MS measurements to obtain a standard curve. Specifically, a five-point calibration curve was created using a purchased Au standard, which yielded an R^2 value of 0.9999.

2.3 TEM images of the AuNPs in the heart

Portions of heart tissues were separated from the heart, cut into 1–1.5 mm^3 pieces, and washed three times with PBS. After prefixation in a 2.5% solution of glutaraldehyde overnight, samples were fixed in 1% phosphate-buffered OsO_4 for 3 h, and dehydrated through graded ethanol solutions of 30%, 50%, 70%, 85%, 95%, and 100% for 7 min each. Then the samples were washed with acetone three times, embedded with resin, and dried in an incubator under the following conditions: 37 ˚C for 12 h, 45 ˚C for 12 h, and 60 ˚C for 48 h. Ultra-thin sections (60 nm thick) were sliced using an ultramicrotome (Leica EM UC7), and stained with uranyl acetate and lead citrate. Finally, imaging was performed using a transmission electron microscope (TEM, Hitachi, H-7500).

2.4 Statistical analysis

The Au content of each tissue at each time point was represented as the means ± standard deviations (S.D.). Student's *t*-tests were used for comparisons between each group, with $p < 0.05$ being considered statistically significant.

The ISI:IVI ratio of the AuNP concentration in each organ was calculated as follows: Each organ and blood AuNP content after ISI divided by the average organ and blood AuNP content after IVI, and the averages of them were calculated.

The relative distribution proportion (P) of the AuNPs in each of the above-mentioned organs was calculated using Eq. (1) as seen below

$$P(\%) = (N_{organ}/N_{total}) \times 100 \quad (1)$$

where N_{organ} is the concentration of AuNPs in an isolated organ, multiplied by the weight of the respective organ; and N_{total} is the sum of N_{organ} for all organs, including the liver, spleen, heart, lungs, intestines, and kidneys.

3 Results and discussion

3.1 Characterization of the AuNPs

The AuNPs had a spherical morphology with a narrow particle size distribution as shown by TEM (see Fig. 2(a)). Their size was uniform, averaging 10.95 ± 0.03 nm as determined from 100 nanoparticles (Fig. 2(b)).

3.2 The Au content in the blood after ISI and IVI

We first investigated the Au content in the blood of the IVI-injected rats. As shown in Fig. 3(a) and Table S1 in the Electronic Supplementary Material (ESM), the Au content drastically decreased between 5 and 15 min ($p < 0.05$) after injection, and gradually decreased thereafter through 24 h after the injection. As shown in Fig. 3(b), the Au content in the blood was only 1.7 ± 1.7 ng·g^{-1} at 5 min after ISI, and no further significant increase or decrease was observed at 1 h after the injection (1.2 ± 0.90 ng·g^{-1}, $p > 0.05$). However, Au content decreased to 0.22 ± 0.09 ng·g^{-1} at 24 h after the injection.

The ISI:IVI was used to show the ratio of the Au content after ISI to that after IVI in different organs to help us more readily evaluate if all of the AuNPs in the organs were diffused from the circulation after ISI. In the blood, the ISI:IVI Au content ratio was 3.9 × 10^{-3} at 5 min after injection (see Fig. 5), indicating that the AuNP content in the blood after ISI was three orders lower than that after IVI. At 15 min after injection, the ratio was 0.022, and progressively increased up to 0.23 at 24 h after injection, indicating that the two administration routes yielded a similar AuNP concentration in the blood after 24 h.

3.3 The *in vivo* biodistribution of the AuNPs in the liver and spleen after ISI and IVI

Five minutes after IVI, the AuNPs that had already transferred into the tissues were analyzed. The highest accumulation of AuNPs was observed in the liver (1,371.4 ± 986.1 ng·g^{-1}, see Fig. 4(a) and Table S2 in the

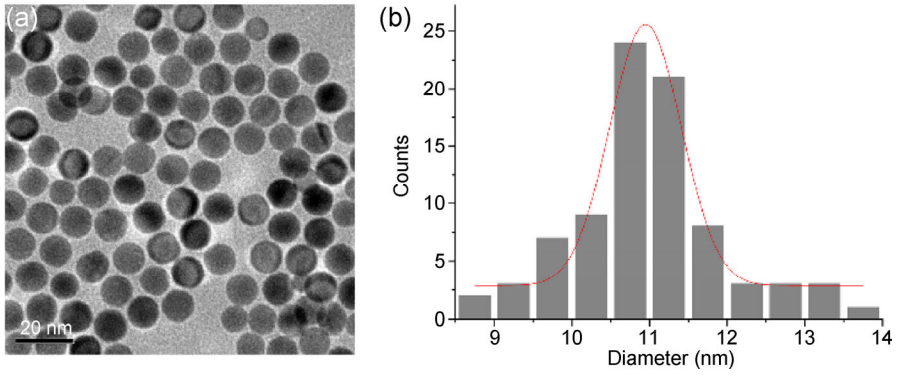

Figure 2 (a) TEM images of AuNPs, and (b) AuNP Gaussian size distribution histograms.

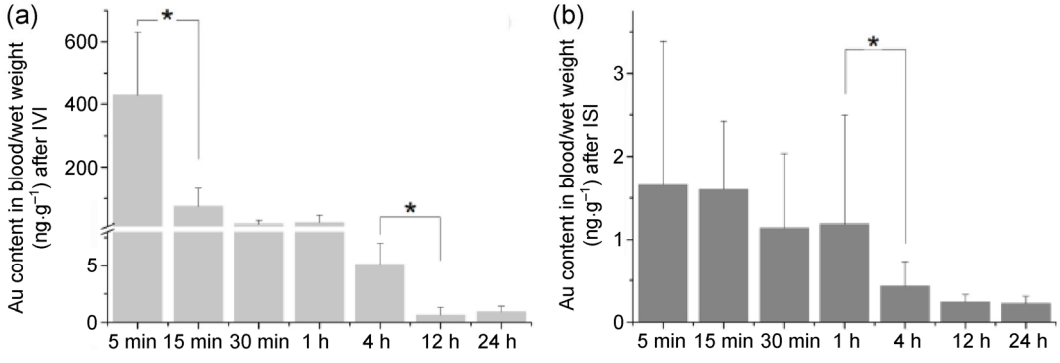

Figure 3 The biodistribution of AuNPs in the blood of SD rats at 5 min, 15 min, 30 min, 1 h, 4 h, 12 h, and 24 h after (a) IVI into the femoral vein and (b) ISI into the tarsal tunnel as determined by ICP-MS.

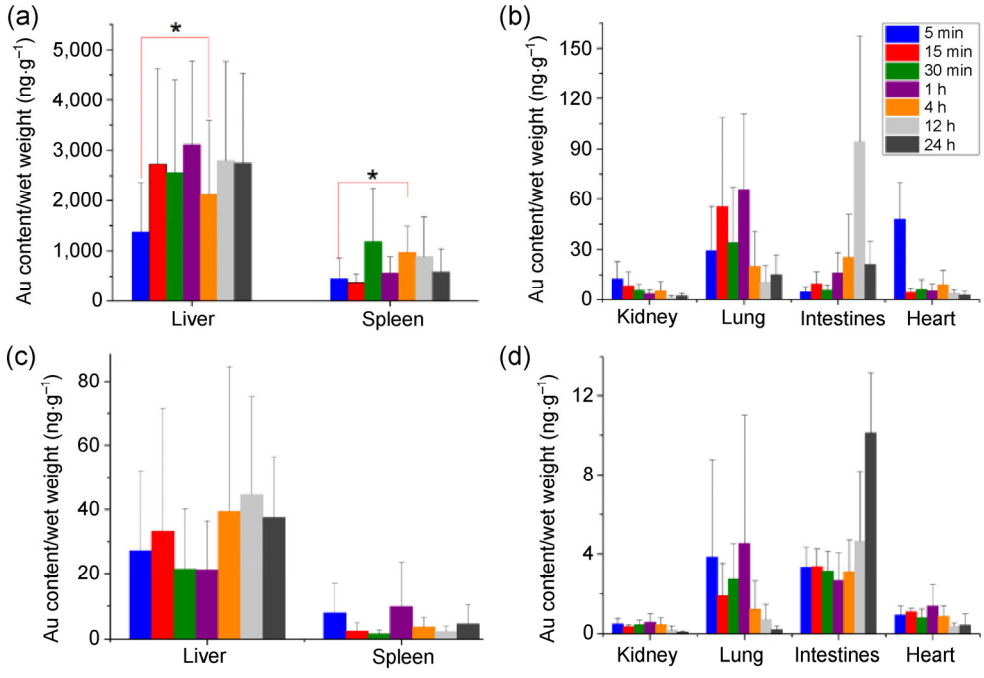

Figure 4 The biodistribution of AuNPs in the liver, spleen, kidneys, lungs, intestines, and heart of SD rats at 5 min, 15 min, 30 min, 1 h, 4 h, 12 h, and 24 h after IVI ((a) and (b)) and ISI in the tarsal tunnel ((c) and (d)) as determined by ICP-MS. The data are represented as the means ± S.D. (a) and (c) The AuNP concentration in the liver and spleen. (b) and (d) The AuNP concentration in the kidneys, lungs, intestines, and heart.

ESM). The content of Au in the liver was significantly and time dependently increased during the first hour after IVI ($p < 0.05$), but did not significantly increase thereafter.

The spleen, another component of the reticuloendothelial system, exhibited the second highest AuNP uptake (see Fig. 4(a) and Table S2 in the ESM). In the spleen, the AuNP content was significantly increased during the first 4 h after IVI ($p < 0.05$), and was slightly, but not significantly, decreased thereafter, measuring 588.9 ± 456.7 ng·g^{-1} AuNP at 24 h after injection.

Figure 4(c) and Table S2 in the ESM show the concentrations of AuNPs in the liver and spleen after ISI. At 5 min after ISI, only 27.2 ± 24.9 ng·g^{-1} AuNP was measured in the liver, without any further significant increase or decrease during the following 24 h ($p > 0.05$). Similarly, the AuNP content in the spleen was not significantly different among the time points measured (2.4 ± 2.3 and 2.2 ± 2.5 ng·g^{-1} at 15 min and 12 h, respectively).

The liver and spleen ISI:IVI Au content ratio was considerably low, measuring 0.021 and 0.014 in the liver, and 0.0049 and 0.0077 in the spleen at 5 min and 24 h after injection, respectively, without any significant changes (Fig. 5(a)).

3.4 The AuNP concentrations in the heart, lungs, intestines, and kidneys

The AuNP biodistribution in the heart, lungs, intestines, and kidneys after ISI and IVI was significantly different from the high accumulation measured in the liver and spleen (see Figs. 4(b) and 4(d), and Table S3 in the ESM). Following IVI, the initial content of AuNPs in the intestines at 5 min after injection (4.5 ± 3.1 ng·g^{-1}) was increased by approximately two-fold at 15 min (9.6 ± 7.3 ng·g^{-1}), and increased to 94.1 ± 63.2 ng·g^{-1} at 12 h after injection. However, after 24 h, the content was decreased to 21.2 ± 13.8 ng·g^{-1}. Following ISI, the initial content of intestinal AuNPs was 3.3 ± 1.0 ng·g^{-1} at 5 min after injection, which was similar to that after IVI. However, no significant differences in AuNP content were observed among the time points measured during the first hour (3.4 ± 0.87 ng·g^{-1}, 3.1 ± 1.0 ng·g^{-1}, 2.6 ± 1.4 ng·g^{-1}, at 15 min, 30 min, and 1 h after injection, respectively). Thereafter, the AuNP uptake gradually

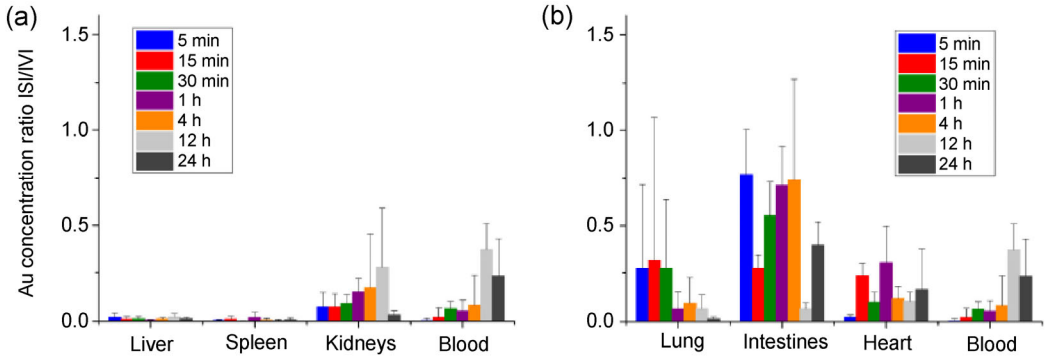

Figure 5 The ISI:IVI ratio of the AuNP concentration in the liver, spleen, kidneys, lungs, intestines, and heart of SD rats at 5 min, 15 min, 30 min, 1 h, 4 h, 12 h, and 24 h after injection.

and time-dependently increased to 10.1 ± 3.0 ng·g^{-1} at 24 h after injection.

The AuNP content in the lungs after IVI increased during the first hour after injection (29.3 ± 26.4 to 65.7 ± 45.0 ng·g^{-1}), and decreased thereafter (15.0 ± 11.8 ng·g^{-1} at 24 h after injection). In contrast, after ISI, the AuNP content was 3.9 ± 4.9 and 0.22 ± 0.17 ng·g^{-1} at 5 min and 24 h after injection, respectively.

The AuNP content in the kidneys exhibited a time-dependent decrease after IVI (12.4 ± 10.4, 3.5 ± 2.5, and 2.0 ± 1.8 ng·g^{-1} at 5 min, 1 h, and 24 h after injection, respectively). However, after ISI, the AuNP content did not significantly change over time (0.49 ± 0.29, 0.46 ± 0.23, and 0.46 ± 0.35 ng·g^{-1} at 5 min, 30 min, and 4 h after injection, respectively). After that, AuNP content in the kidneys was reduced to 0.19 ± 0.20 and 0.091 ± 0.059 ng·g^{-1} at 12 h and 24 h after injection, respectively.

Some AuNP uptake was observed in the heart, both after IVI and ISI. After IVI, the AuNP content in the heart was 47.9 ± 22.1, 4.2 ± 2.6, and 2.6 ± 2.3 ng·g^{-1} at 5 min, 15 min, and 24 h after injection, respectively. Distinct from that after IVI, the AuNP concentration in the heart after ISI maintained a similar level during the first four hours after injection (0.94 ± 0.43, 0.80 ± 0.42, and 0.87 ± 0.52 ng·g^{-1} at 5 min, 30 min, and 4 h, respectively), but was decreased to 0.43 ± 0.57 ng·g^{-1} at 24 h after injection.

Although the AuNP content in the blood after ISI was significantly less than that after IVI, the AuNP uptake into some of the organs investigated was highly similar between the two injection routes. Therefore, we used the ISI:IVI ratio of the Au content to evaluate the observed differences. As shown in Fig. 5, at 5 min after injection, the ratios were approximately 0.27 and 0.77 for the lungs and intestines, respectively, which were two orders of magnitude higher than those for the blood at the same time point. The ISI:IVI ratios for the heart and the kidneys (0.024 and 0.074, respectively) were one order of magnitude higher than that for the blood (0.0039) at 5 min after injection. At 15 min after injection, the ratio increased to 0.24 for the heart, which was also one order of magnitude higher than that for the blood (0.022). The ISI:IVI ratio of the Au content for the intestines remained high (0.74) at 4 h after injection, which was also far higher than that for the blood (0.084).

We also calculated the relative distribution proportion of AuNP content in the analyzed organs, excluding the liver because of its too high AuNP content and weight compared to those of the other organs (see Fig. 6). Relatively higher amounts of AuNPs were observed in some organs at the earlier time points after ISI compared to those after IVI.

To further evaluate whether the AuNPs were transferred to these organs by ISI, we used TEM to observe the dispersal of AuNPs in the heart, as an example, with physiological saline injection as a control. As shown in Fig. 7, there were some ultra-structures with loose connective tissues seen as fibrils (green arrows) or bundles of fibrils (orange arrows). After injection of AuNPs, we found that some AuNPs (red arrows) were distributed within the loose connective tissues (see Figs. 7(c) and 7(d)).

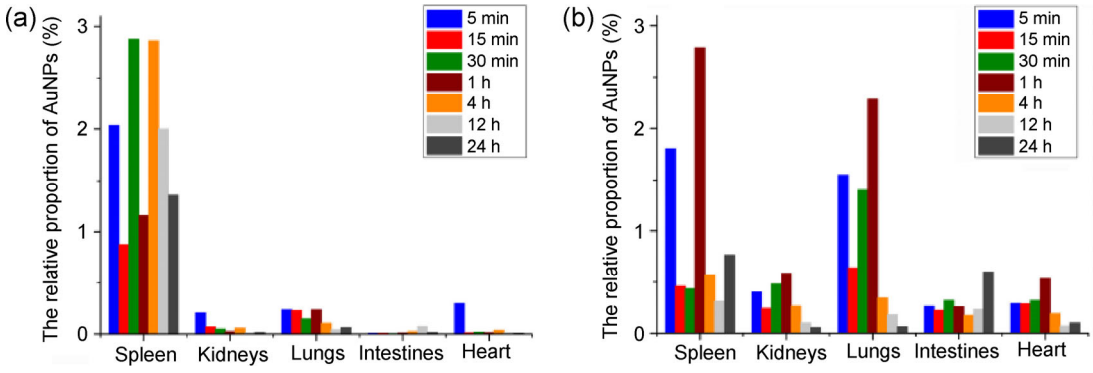

Figure 6 The relative distribution proportion of the AuNPs in the spleen, kidneys, lungs, intestines, and heart of SD rats at 5 min, 15 min, 30 min, 1 h, 4 h, 12 h, and 24 h after IVI (a), and after ISI in the tarsal tunnel (b).

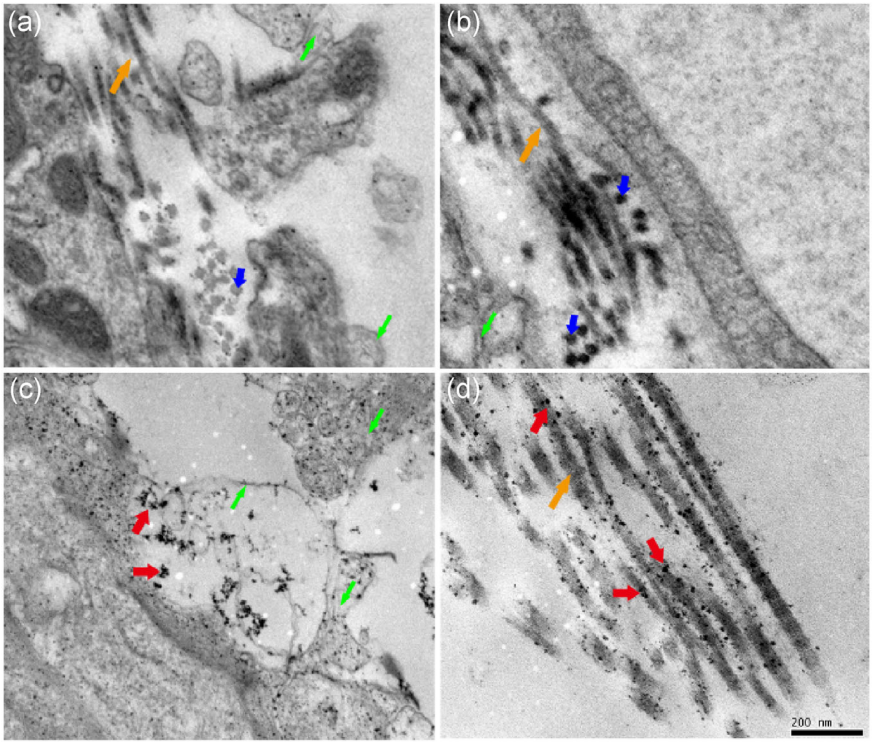

Figure 7 TEM images of the AuNPs in the heart of a SD rat at 1 h after ISI in the tarsal tunnel. (a) and (b) TEM images after injection of physiological saline as a control. (c) and (d) TEM images after injection of AuNPs (red arrow: AuNPs; green arrow: fibrils; orange arrow: bundle of fibrils; blue arrow: cross section of fibrils).

3.5 The biodistribution of the AuNPs in the skin and muscle

In addition to the viscera, we also investigated the biodistribution of the AuNPs in the skin and muscle (rectus femoris) of the right tibia of the leg contralateral to that injected with the AuNPs. As shown in Fig. 8, there was a distinct distribution pattern of AuNPs in the muscle and skin at each time point measured after ISI and IVI. Specifically, the AuNP content in the muscle slowly decreased in a time-dependent manner after IVI, while after ISI, it increased from 13.3 ± 17.1 to 23.4 ± 22.8 ng·g^{-1} during the first 15 min, and then decreased over time to 1.3 ± 0.28 ng·g^{-1} at 24 h after injection. Although the content of AuNPs in the blood after ISI was considerably lower than

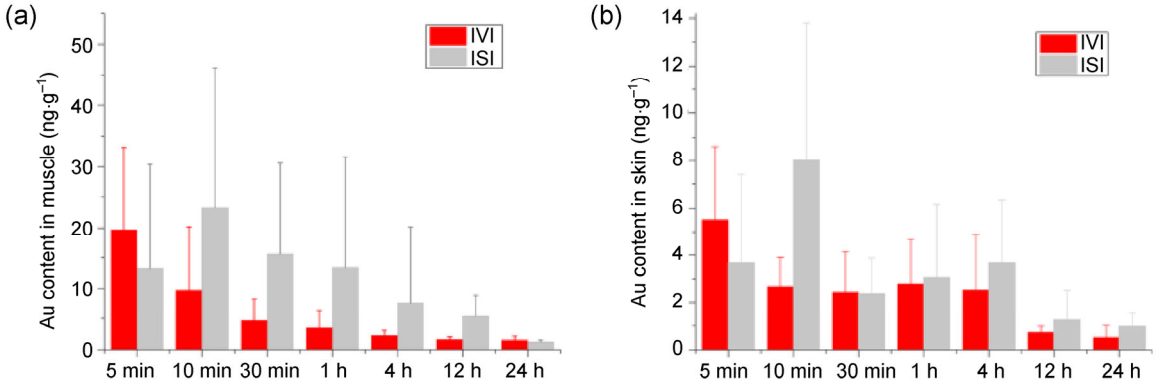

Figure 8 The biodistribution of the AuNPs in the muscle (a) and skin (b) of SD rats at 5 min, 15 min, 30 min, 1 h, 4 h, 12 h, and 24 h after IVI and ISI in the tarsal tunnel as determined by ICP-MS.

that after IVI, the content in the muscle and skin after ISI was higher than that after IVI, except at 5 min after injection.

In the current study, we investigated the biodistribution and transport of AuNPs in rats after ISI or IVI. Although AuNPs have potential applications in diverse biomedical fields because of their specific properties [22–24], data and the respective conclusions drawn from them regarding the levels and kinetics of NP biodistribution have been inconsistent because of differences in NP properties, doses, and administration routes [9, 25, 26].

There are several different routes for administration of NPs into living biological systems, which is followed by their distribution to the organs and tissues via the circulation as their main transport pathway [27]. Among the various administration routes, IVI is most commonly used in many experimental settings because of the direct administration into the circulation [28, 29].

Following IVI, most NPs are removed from the circulation and have been subsequently observed in mononuclear phagocytes in the liver and spleen for long periods of time [14, 30–32], which is in agreement with the results of the current study. Our results showed that the injected AuNPs had a very fast clearance rate in the blood. Approximately 98% and 1% of the AuNPs accumulated in the liver and spleen, respectively, whereas the AuNP accumulation in the other four organs was less than 1% at all time points measured.

Our results demonstrated that the AuNP distribution to the analyzed organs was highly different between the ISI and IVI administration routes. The AuNP content in the blood was considerably lower after ISI than after IVI at all time points measured. This suggests that the retrograde transfer of AuNPs from the peripheral tissues into the circulation is hampered by the relatively weaker diffusion ability of the AuNPs compared to that of small molecules.

Interestingly, the distribution of AuNPs at certain time points was similar in some of the tissues analyzed. For example, the AuNP content in the intestines was 3.3 ± 1.0 ng·g^{-1} after ISI compared to 4.5 ± 3.1 ng·g^{-1} after IVI at 5 min after injection. At 15 min after injection, the AuNP concentration in the heart was approximately 4.2 ± 2.6 ng·g^{-1} after IVI and 1.1 ± 0.14 ng·g^{-1} after ISI. In the skin and muscle, the AuNP concentration after ISI was even higher than that after IVI at some of the time points measured. These phenomena were further demonstrated by the ISI:IVI ratio and the relative distribution proportion of the AuNP concentration. The ISI:IVI ratio for the blood was only 0.0039 at the 5 min time point, but was 0.77 and 0.27 for the intestines and lungs, respectively. For the heart, the ISI:IVI ratio was approximately 0.24, but was only 0.022 for the blood at the 15 min time point. Importantly, the relative distribution proportion of the AuNPs in the intestines, heart, and lungs was considerably higher after ISI than after IVI at the early time points measured.

The prior results suggested the existence of fast,

direct AuNP transport pathways to the organs. It is generally believed that, after their initial absorption, NPs migrate into the circulation first, and are subsequently distributed to most organs and tissues in the body [27]. However, in the current study, the distribution of the AuNPs in the blood after ISI at the time points measured was much lower than that after IVI. If the AuNPs had been transferred to the analyzed tissues via the blood, then their distribution to these organs after ISI should also have been much lower than that after IVI. Therefore, due to the results of our experiments, we speculated that the observed fast AuNP transport to the organs was not via the circulation.

Indeed, pathways other than the circulation are believed to be involved in the biodistribution of NPs [33, 34]. For example, Edler et al. exposed rats to ultrafine manganese oxide particles via the nostrils and found that the NPs were translocated to the central nervous system via the olfactory neuronal pathway [33]. Iliff et al. described an anatomically distinct clearing system in a paravascular compartment between the outside of blood vessels and astrocytic endfeet in the brain, which served as a lymphatic-like mechanism that resorbed interstitial fluid, selectively transported small lipid molecules, and could act as a signaling route for astrocyte communication [35, 36]. Carare et al. also found that soluble tracers initially spread diffusely through the brain parenchyma, and subsequently left the brain parenchyma along the basement membranes of cerebral capillaries and arteries [37]. These novel transport phenomena suggest that some structures exist in living biological systems that may support the transport and biodistribution behaviors observed in the current study.

Although the anatomical and histological structures involved in mammalian physiology have been well characterized, novel structures are still being discovered [38]. Our previous work demonstrated the existence of a potential drainage system comprising loose connective tissues separate from the blood or lymphatic vessels [17–19]. Loose connective tissues can be found in almost every part of the body, and form a complex connective tissue network system. They surround and infiltrate tissues to form specific structural characteristics in muscles and organs such as the lungs and intestines [19, 39]. The tarsal tunnel we used for the ISI is the depression formed by certain bones, and is occupied by certain tendons, such as those of the flexor digitorum longus, the tibialis posterior, and the flexor hallucis longus, which comprise of the connective tissue [21]. Our study found that NPs could migrate rapidly to certain organs in several minutes after ISI. This new discovery of a long-range transport route of NPs by loose connective tissues provides novel insight into the biodistribution and transport of NPs *in vivo*.

Loose connective tissues may also be regarded as hierarchical multiphase porous systems. Since the NPs were translocated rapidly into different biological tissues via this unique transport and distribution system, it follows that a novel mechanism of long-range transport may exist. This mechanism may be via the nano-confined air/water/solid interface inside or outside the cells in living biological systems. Along these lines, a single cell, the extracellular matrix with specific structural characteristics, and even a whole organism may be recognized as a whole system consisting of typical multiphase porous structures with nano-confined air/water/solid interfaces.

These results contribute to a deeper understanding of physiological and pathological processes in living biological systems, as biomolecules such as growth factors and enzymes may be distributed via this pathway. This alternative distribution route may regulate physiological functions such as the regulation of blood vessel wall nutrition, and suggest a mechanism by which acupuncture may influence health.

As a new biodistribution pathway, the mechanism described herein may provide a more specific nanoscale drug delivery system to target diseased tissues and avoid distribution to systemic circulation. Current thinking suggests that after initial NP absorption, NPs migrate into the circulation first, and subsequently distribute to the tissues and organs, which makes the NPs capable of only passive targeting. Moreover, after the NPs enter the blood, their surfaces are readily covered by selective blood plasma proteins forming a protein corona that can influence the properties of NPs and change their biodistribution in the body.

This is a disadvantage of NPs as it affects their stability, targeting, and controlled release. After ISI, NPs were rapidly transferred to certain organs, including the heart, intestines, and lungs, though not via systemic circulation. This may lead to novel NP injection strategies as active NP targeting preparations could avoid interactions with blood plasma proteins and distribution to the circulation. However, the exact mechanisms underlying this pathway are not yet understood. Therefore, further studies to evaluate the effects of NP properties, such as size, shape, surface functionalization, and charge, on transport via this pathway are warranted.

4 Conclusions

Our results herein showed that a clearly different transport and biodistribution pathway for AuNPs exists between the ISI and IVI administration routes. The distribution proportion of the AuNPs to the skin, muscle, heart, intestines, and lungs at the early time points measured was higher after ISI than after IVI. Therefore, we postulate that the distribution of AuNPs to some organs is mediated not via the circulation, but rather via loose connective tissues, which exist in almost every part of the body and form a complex network system. Our results provide novel evidence for the existence of this alternative NP transport mechanism, contribute to a deeper understanding of physiological and pathological processes involving biodistribution, and may facilitate the development of nanoscale drug delivery strategies to several different organisms.

Acknowledgements

This work was supported by the National Basic Research Program of China (Nos. 2015CB5545507 and 2013CB933700) and the National Natural Science Foundation of China (No. 21305024).

Electronic Supplementary Material: Supplementary material (Table S1: the AuNP content ($ng \cdot g^{-1}$) in the blood after IVI and ISI as measured by ICP-MS; Table S2: the AuNP content ($ng \cdot g^{-1}$) in the liver and spleen at different time points after IVI and ISI as measured by ICP-MS; Table S3: the AuNP content ($ng \cdot g^{-1}$) in the intestines, lungs, heart, and kidneys at different time points after IVI and ISI as measured by ICP-MS) is available in the online version of this article at http://dx.doi.org/10.1007/s12274-016-1100-3.

References

[1] Mahmoudi, M.; Sant, S.; Wang, B.; Laurent, S.; Sen, T. Superparamagnetic iron oxide nanoparticles (SPIONs): Development, surface modification and applications in chemotherapy. *Adv. Drug Deliv. Rev.* **2011**, *63*, 24–46.

[2] Liu, Y.; Chen, C. Y.; Qian, P. X.; Lu, X. F.; Sun, B. Y.; Zhang, X.; Wang, L. M.; Gao, X. F.; Li, H.; Chen, Z. Y. et al. Gd-metallofullerenol nanomaterial as non-toxic breast cancer stem cell-specific inhibitor. *Nat. Commun.* **2015**, *6*, 5988.

[3] Xiao, X. L.; Lu, J.; Li, Y. D. $LiMn_2O_4$ microspheres: Synthesis, characterization and use as a cathode in lithium ion batteries. *Nano Res.* **2010**, *3*, 733–737.

[4] Cobley, C. M.; Chen, J. Y.; Cho, E. C.; Wang, L. V.; Xia, Y. N. Gold nanostructures: A class of multifunctional materials for biomedical applications. *Chem. Soc. Rev.* **2011**, *40*, 44–56.

[5] Wang, P. P.; Yu, Q. Y.; Long, Y.; Hu, S.; Zhuang, J.; Wang, X. Multivalent assembly of ultrasmall nanoparticles: One-, two-, and three-dimensional architectures of 2 nm gold nanoparticles. *Nano Res.* **2012**, *5*, 283–291.

[6] Dreaden, E. C.; Mackey, M. A.; Huang, X. H.; Kang, B.; El-Sayed, M. A. Beating cancer in multiple ways using nanogold. *Chem. Soc. Rev.* **2011**, *40*, 3391–3404.

[7] Dobrovolskaia, M. A.; McNeil, S. E. Immunological properties of engineered nanomaterials. *Nat. Nanotechnol.* **2007**, *2*, 469–478.

[8] Chen, P. C.; Mwakwari, S. C.; Oyelere, A. K. Gold nanoparticles: From nano medicine to nanosensing. *Nanotechnol. Sci. Appl.* **2008**, *1*, 45–65.

[9] Khlebtsov, N.; Dykman, L. Biodistribution and toxicity of engineered gold nanoparticles: A review of *in vitro* and *in vivo* studies. *Chem. Soc. Rev.* **2011**, *40*, 1647–1671.

[10] Yah, C. S.; Simate, G. S.; Iyuke, S. E. Nanoparticles toxicity and their routes of exposures. *Pak. J. Pharm. Sci.* **2012**, *25*, 477–491.

[11] Yah, C. S. The toxicity of gold nanoparticles in relation to their physiochemical properties. *Biomed. Res.* **2013**, *24*, 400–413.

[12] De Jong, W. H.; Hagens, W. I.; Krystek, P.; Burger, M. C.;

Sips, A. J. A. M.; Geertsma, R. E. Particle size-dependent organ distribution of gold nanoparticles after intravenous administration. *Biomaterials* **2008**, *29*, 1912–1919.

[13] Zhang, X. D.; Wu, H. Y.; Wu, D.; Wang, Y. Y.; Chang, J. H.; Zhai, Z. B.; Meng, A. M.; Liu, P. X.; Zhang, L. A.; Fan, F. Y. Toxicologic effects of gold nanoparticles *in vivo* by different administration routes. *Int. J. Nanomedicine* **2010**, *5*, 771–781.

[14] Wang, L. M.; Li, Y. F.; Zhou, L. J.; Liu, Y.; Meng, L.; Zhang, K.; Wu, X. C.; Zhang, L. L.; Li, B.; Chen, C. Y. Characterization of gold nanorods *in vivo* by integrated analytical techniques: Their uptake, retention, and chemical forms. *Anal. Bioanal. Chem.* **2010**, *396*, 1105–1114.

[15] Hillyer, J. F.; Albrecht, R. M. Gastrointestinal persorption and tissue distribution of differently sized colloidal gold nanoparticles. *J. Pharm. Sci.* **2001**, *90*, 1927–36.

[16] Sharifi, S.; Behzadi, S.; Laurent, S.; Forrest, M. L.; Stroeve, P.; Mahmoudi, M. Toxicity of nanomaterials. *Chem. Soc. Rev.* **2012**, *41*, 2323–2343.

[17] Li, H. Y.; Chen, M.; Yang, J. F.; Yang, C. Q.; Xu, L.; Wang, F.; Tong, J. B.; Lv, Y.; Suonan, C. Fluid flow along venous adventitia in rabbits: Is it a potential drainage system complementary to vascular circulations? *PLoS One* **2012**, *7*, e41395.

[18] Li, H. Y.; Tong, J. B.; Cao, W. G.; Chen, M.; Li, H.; Dai, H.; Xu, L.; Chen, X. L. Longitudinal non-vascular transport pathways originating from acupuncture points in extremities visualised in human body. *Chin. Sci. Bull.* **2014**, *59*, 5090–5095.

[19] Feng, J. T.; Wang, F.; Han, X. X.; Ao, Z.; Sun, Q. M.; Hua, W. D.; Chen, P. P.; Jing, T. W.; Li, H. Y.; Han, D. A "green pathway" different from simple diffusion in soft matter: Fast molecular transport within micro/nanoscale multiphase porous systems. *Nano Res.* **2014**, *7*, 434–442.

[20] Ma, Y. Y.; Li, W. Y.; Cho, E. C.; Li, Z. Y.; Yu, T.; Zeng, J.; Xie, Z. X.; Xia, Y. N. Au@Ag core-shell nanocubes with finely tuned and well-controlled sizes, shell thicknesses, and optical properties. *ACS Nano* **2010**, *4*, 6725–6734.

[21] Drake, R. L.; Vogl, W.; Mitchell, A. W. M. *Gray's Anatomy for Students*; Elsevier: Philadelphia, 2005.

[22] Boisselier, E.; Astruc, D. Gold nanoparticles in nanomedicine: Preparations, imaging, diagnostics, therapies and toxicity. *Chem. Soc. Rev.* **2009**, *38*, 1759–1782.

[23] Jiang, Y. Y.; Deng, Z. J.; Yang, D.; Deng, X.; Li, Q.; Sha, Y. L.; Li, C. H.; Xu, D. S. Gold nanoflowers for 3D volumetric molecular imaging of tumors by photoacoustic tomography. *Nano Res.* **2015**, *8*, 2152–2161.

[24] Howes, P. D.; Chandrawati, R.; Stevens, M. M. Colloidal nanoparticles as advanced biological sensors. *Science* **2014**, *346*, 1247390.

[25] Ng, V. W. K.; Berti, R.; Lesage, F.; Kakkar, A. Gold: A versatile tool for *in vivo* imaging. *J. Mater. Chem. B* **2013**, *1*, 9–25.

[26] Schleh, C.; Semmler-Behnke, M.; Lipka, J.; Wenk, A.; Hirn, S.; Schäffler, M.; Schmid, G.; Simon, U.; Kreyling, W. G. Size and surface charge of gold nanoparticles determine absorption across intestinal barriers and accumulation in secondary target organs after oral administration. *Nanotoxicology* **2012**, *6*, 36–46.

[27] Hagens, W. I.; Oomen, A. G.; de Jong, W. H.; Cassee, F. R.; Sips, A. J. A. M. What do we (need to) know about the kinetic properties of nanoparticles in the body? *Regul. Toxicol. Pharmacol.* **2007**, *49*, 217–229.

[28] Koo, H.; Huh, M. S.; Sun, I. C.; Yuk, S. H.; Choi, K.; Kim, K.; Kwon, I. C. *In vivo* targeted delivery of nanoparticles for theranosis. *Acc. Chem. Res*. **2011**, *44*, 1018–1028.

[29] Park, K.; Lee, S.; Kang, E.; Kim, K.; Choi, K.; Kwon, I. C. New generation of multifunctional nanoparticles for cancer imaging and therapy. *Adv. Funct. Mater.* **2009**, *19*, 1553–1566.

[30] Semmler-Behnke, M.; Kreyling, W. G.; Lipka, J.; Fertsch, S.; Wenk, A.; Takenaka, S.; Schmid, G.; Brandau, W. Biodistribution of 1.4- and 18-nm gold particles in rats. *Small* **2008**, *4*, 2108–2111.

[31] Balasubramanian, S. K.; Jittiwat, J.; Manikandan, J.; Ong, C. N.; Yu, L. E.; Ong, W. Y. Biodistribution of gold nanoparticles and gene expression changes in the liver and spleen after intravenous administration in rats. *Biomaterials* **2010**, *31*, 2034–2042.

[32] Choi, C. H. J.; Alabi, C. A.; Webster, P.; Davis, M. E. Mechanism of active targeting in solid tumors with transferrin-containing gold nanoparticles. *Proc. Natl. Acad. Sci. USA* **2010**, *107*, 1235–1240.

[33] Elder, A.; Gelein, R.; Silva, V.; Feikert, T.; Opanashuk, L.; Carter, J.; Potter, R.; Maynard, A.; Ito, Y.; Finkelstein, J. et al. Translocation of inhaled ultrafine manganese oxide particles to the central nervous system. *Environ. Health Perspect.* **2006**, *114*, 1172–1178.

[34] Matsui, Y.; Sakai, N.; Tsuda, A.; Terada, Y.; Takaoka, M.; Fujimaki, H.; Uchiyama, I. Tracking the pathway of diesel exhaust particles from the nose to the brain by X-ray florescence analysis. *Spectrochim. Acta B* **2009**, *64*, 796–801.

[35] Iliff, J. J.; Wang, M.; Liao, Y.; Plogg, B. A.; Peng, W.; Gundersen, G. A.; Benveniste, H.; Vates, G. E.; Deane, R.; Goldman, S. A. et al. A paravascular pathway facilitates CSF flow through the brain parenchyma and the clearance

of interstitial solutes, including amyloid β. *Sci. Transl. Med.* **2012**, *4*, 147ra111.

[36] Thrane, V. R.; Thrane, A. S.; Plog, B. A.; Thiyagarajan, M.; Iliff, J. J.; Deane, R.; Nagelhus, E. A.; Nedergaard, M. Paravascular microcirculation facilitates rapid lipid transport and astrocyte signaling in the brain. *Sci. Rep.* **2013**, *3*, 2582.

[37] Carare, R. O.; Bernardes-Silva, M.; Newman, T. A.; Page, A. M.; Nicoll, J. A. R.; Perry, V. H.; Weller, R. O. Solutes, but not cells, drain from the brain parenchyma along basement membranes of capillaries and arteries: Significance for cerebral amyloid angiopathy and neuroimmunology. *Neuropathol. Appl. Neurobiol.* **2008**, *34*, 131–144.

[38] Louveau, A.; Smirnov, I.; Keyes, T. J.; Eccles, J. D.; Rouhani, S. J.; Peske, J. D.; Derecki, N. C.; Castle, D.; Mandell, J. W.; Lee, K. S. et al. Structural and functional features of central nervous system lymphatic vessels. *Nature* **2015**, *523*, 337–341.

[39] Langevin, H. M. Connective tissue: A body-wide signaling network? *Med. Hypotheses* **2006**, *66*, 1074–1077.